American Mineralogist, Volume 95, pages 392–396, 2010

Galliskiite, $Ca_4Al_2(PO_4)_2F_8 \cdot 5H_2O$, a new mineral from the Gigante granitic pegmatite, Córdoba province, Argentina

Anthony R. Kampf,[1,*] Fernando Colombo,[2] William B. Simmons,[3] Alexander U. Falster,[3] and James W. Nizamoff[3,†]

[1]Mineral Sciences Department, Natural History Museum of Los Angeles County, 900 Exposition Blvd., Los Angeles, California 90007, U.S.A.
[2]CONICET, Cátedra de Geología General, Facultad de Ciencias Exactas, Físicas y Naturales, Pabellón Geología, Universidad Nacional de Córdoba, Vélez Sarsfield 1611, (X5016GCA) Córdoba, Argentina
[3]Department of Earth and Environmental Science, University of New Orleans, 2000 Lakeshore Drive, New Orleans, Louisiana 70148, U.S.A.

Abstract

Galliskiite, ideally $Ca_4Al_2(PO_4)_2F_8 \cdot 5H_2O$, is a new mineral found at the Gigante granitic pegmatite, Punilla department, Córdoba Province, Argentina. It is named for Argentine mineralogist and pegmatite specialist Miguel Ángel Galliski. Galliskiite is triclinic, $P\bar{1}$, $a = 6.1933(7)$, $b = 9.871(1)$, $c = 13.580(2)$ Å, $\alpha = 89.716(3)$, $\beta = 75.303(4)$, $\gamma = 88.683(4)°$, $Z = 2$. The strongest lines in the X-ray powder diffraction pattern are [*d* in Å, (*I*)]: 7.904 (70), 5.994 (100), 3.280 (58), 3.113 (30), 2.945 (85), 2.887 (44), 2.483 (20), 2.262 (27), 2.150 (23), 1.821 (27), and 1.798 (25). It occurs as crude platy crystals elongated along [001] and flattened on {010}, with frosty surfaces. Simple contact and polysynthetic twinning on {100} by rotation about [010] is ubiquitous. It is colorless and transparent, has white streak and vitreous luster, and is nonfluorescent under ultraviolet radiation. It has a Mohs hardness of 2½, conchoidal to irregular fracture and two fair cleavages at approximately 90°. The measured density is 2.67(3) g/cm^3, and the calculated density is 2.670 g/cm^3. Galliskiite dissolves slowly in concentrated HCl. The mineral is biaxial (+), $\alpha = 1.493(1)$, $\beta = 1.495(1)$, $\gamma = 1.520(1)$, $2V_{meas} = 33(5)°$, $2V_{calc} = 32°$; dispersion, $r < v$; orientation $Z \approx$ **b**, *X* and *Z* at 40–50° from **a** and **c**. No pleochroism is observed. Analysis by electron microprobe (average of 12 analyses given in wt%) provided CaO 34.71, MgO 0.01, FeO 0.10, MnO 0.17, Al_2O_3 15.92, SiO_2 0.06, TiO_2 0.01, P_2O_5 21.94, F 21.35, H_2O (calculated by stoichiometry) 15.08, less F≡O 8.99, total 100.39 wt%. The empirical formula, based on 21 (F+O), is $(Ca_{3.98}Mn_{0.02}Fe_{0.01})_{\Sigma 4.0}Al_{2.01}(P_{1.99}Si_{0.01}O_8)F_{7.23}(OH)_{0.77} \cdot 5H_2O$. The crystal structure, solved and refined using single-crystal data to $R_1 = 0.033$, consists of double chains of alternating corner-sharing AlF_3O_3 octahedra and PO_4 tetrahedra along the **a** axis. The chains are joined into a framework via bonds to four distinct Ca atoms. Calcium atoms are also linked by sharing isolated F atoms and H_2O molecules. The double-chain motif in the structure of galliskiite is distinct from that in any other known phosphate.

Keywords: Galliskiite, new mineral, pegmatite phosphate, Córdoba, Argentina

Introduction

The Punilla pegmatite district (Galliski 1999) comprises several intragranitic pegmatites related to the Achala batholith. The parental magma was rich in fluorine (Dorais et al. 1997), and this is reflected, among other features, in the common presence of triplite-zwieselite in the pegmatites, sometimes as meter-sized masses.

In most pegmatites, triplite shows signs of alteration in patches and along cracks, the most common secondary phosphates being bermanite, strengite, and phosphosiderite. Mn-bearing apatite-(CaF) and sulfides (pyrite >> chalcopyrite) usually occur in close proximity to triplite and are also frequently altered, leaving spongy masses where secondary phosphates precipitate.

Despite the economic relevance of pegmatites from the Punilla district, many aspects of their mineralogy remain obscure, and phosphates are no exception. Almost 20 secondary phosphates have been identified, mostly using X-ray powder diffraction, from pegmatites mined at Cerro Blanco (summarized by Colombo et al. 2007), but little information exists on the mineralogy of other bodies. One notable exception is the study on columbite-group minerals (Galliski and Černý 2006).

During an examination of samples collected from the Gigante pegmatite, one of us (J.N.) noticed crystals of a mineral that resembled gypsum. Preliminary EDS analyses showed major Al, Ca, and P (the instrument only detected elements with $Z > 10$), and an X-ray diffraction pattern failed to match any known species. Further studies showed it to be a new mineral (IMA 2009-038) for which the name galliskiite was chosen to honor Miguel Ángel Galliski (b. 1948), Argentine mineralogist and pegmatite specialist whose research on the pegmatites of the Pampean Pegmatite Province of northwestern Argentina (Galliski 1999) has, inter alia, yielded two new minerals, bederite and ferrotitanowodginite (Galliski et al. 1999a, 1999b). Galliski agreed to the naming of the mineral, and the mineral and name have been approved by the Commis-

* E-mail: akampf@nhm.org
† Current address: Omya, Inc., 39 Main Street, Proctor, Vermont 05765, U.S.A.

sion on New Minerals, Nomenclature and Classification of the International Mineralogical Association. The holotype specimen is deposited in the Natural History Museum of Los Angeles County, with catalog number 62500.

Occurrence

The type locality of galliskiite is the Gigante pegmatite, 18.45 km W-SW of the town of Tanti, Punilla department, Córdoba Province, Argentina (Lat. 31°24′31.0″S, Long. 64°46′19.6″W). The most relevant features of this body, genetically related to the Devonian Achala batholith (Lira and Kirschbaum 1990; Rapela et al. 2008), have been summarized by Kampf et al. (2010).

Galliskiite occurs as crystals growing on a drusy layer of morinite covering triplite. Small clusters of pale-pink strengite crystals can be found scattered on the morinite. On the same specimen, galliskiite also forms massive intergrown vein fillings in triplite, but always separated from it by morinite. Clearly galliskiite is a late-stage hydrothermal mineral that crystallized from fluorine-rich solutions. It has compositional similarities with morinite, $NaCa_2Al_2(PO_4)_2(F,OH)_5 \cdot 2H_2O$, which crystallized immediately before it. Another mineral from the Gigante pegmatite with similar chemistry is carlhintzeite, $Ca_2AlF_7 \cdot H_2O$, which occurs on drusy bermanite and is also interpreted as a late-stage hydrothermal phase. Even though carlhintzeite has not been found on the same specimen with galliskiite, its presence in the same general assemblage is further indication of the presence of late-stage hydrothermal fluids rich in Ca, Al, and F. Other hydrothermal or secondary phosphates found in the Gigante pegmatite, but not associated with galliskiite, are apatite-(CaF), childrenite-eosphorite, cyrilovite, fluellite, gayite (Kampf et al. 2010), hentschelite, lacroixite, metatorbernite, and phosphosiderite.

Physical and optical properties

Crystals display a platy habit (Fig. 1), elongated along [001], and flattened on {010}. Forms could not be measured because the crystals are composites with multiply stepped and offset faces giving them a crude shape and frosted appearance. Simple contact and polysynthetic twinning on {100} by rotation about [010] is ubiquitous.

Galliskiite is colorless and transparent, with a white streak. Luster is vitreous on broken surfaces, but crystal faces have a frosted appearance because they are made up of numerous steps and offsets. It does not fluoresce under either short- or long-wave ultraviolet radiation. The Mohs hardness is 2½ (it scratches gypsum, but not calcite). The mineral is brittle and has two fair cleavages at ~90° (probably {010} and {001}). Parting has not been observed, and fracture is conchoidal to irregular. The density, measured by the sink-float method in an aqueous solution of sodium polytungstate, is 2.67(3) g/cm^3, identical to the calculated density (2.670 g/cm^3). Galliskiite dissolves slowly in concentrated HCl.

The new mineral is optically biaxial (+) and nonpleochroic. Its refractive indices (measured in white light) are $\alpha = 1.493(1)$, $\beta = 1.495(1)$, $\gamma = 1.520(1)°$, with moderate $r < v$ dispersion; $2V_{meas} = 33(5)°$, $2V_{calc} = 32°$. The orientation is: $Z \approx \mathbf{b}$, X and Z at 40–50° from **a** and **c**.

Chemical composition

Twelve chemical analyses were carried out using an ARL-SEMQ electron microprobe (WDS mode, 15 kV, 10 nA, 3 μm beam diameter). No direct determination of H_2O was possible due to paucity of material, but its presence was confirmed by crystal-structure analysis. Therefore, the H_2O content was calculated by stoichiometry. Analytical data and standards are given in Table 1. The empirical formula (based on O+F = 21) is $(Ca_{3.98}Mn_{0.02}Fe_{0.01})_{\Sigma 4.01}Al_{2.01}(P_{1.99}Si_{0.01}O_8)F_{7.23}(OH)_{0.77} \cdot 5H_2O$. The simplified formula is $Ca_4Al_2(PO_4)_2F_8 \cdot 5H_2O$, which requires (in wt%) CaO 34.71, Al_2O_3 15.78, P_2O_5 21.96, F 23.52, H_2O 13.94, O≡F –9.90, total 100.00 wt%.

The Gladstone-Dale compatibility index $1 - (K_P/K_C)$ as defined by Mandarino (1981) provides a measure of the consistency

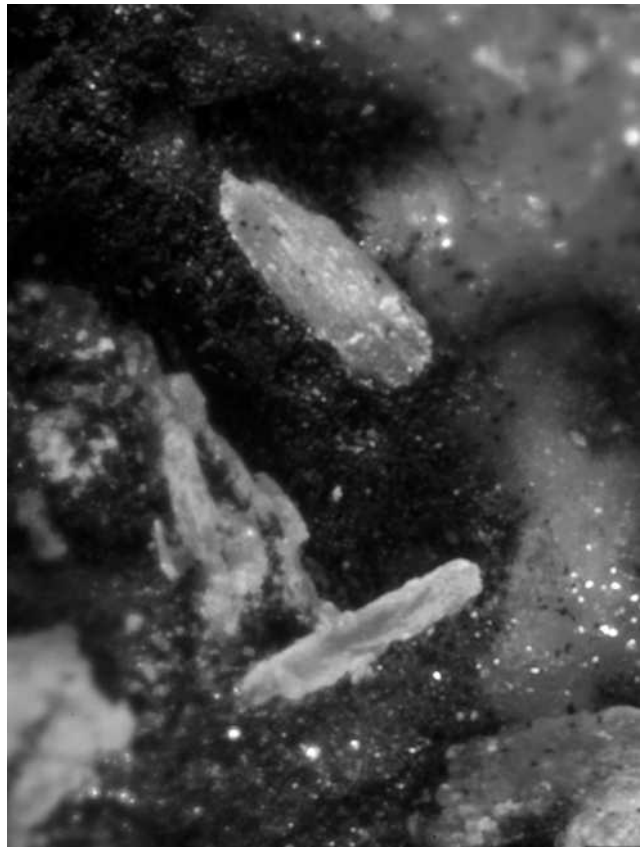

Figure 1. Galliskiite blades up to 0.5 mm in length on colorless druse of morinite with brown-black coating of indistinct Fe-Mn oxides.

Table 1. Analytical data for galliskiite (average of 12 electron-microprobe analyses)

Constituent	wt%	Range	St. dev.	Standard
CaO	34.71	34.22–35.05	0.21	apatite-(CaF)
MgO	0.01	0.00–0.02	0.01	periclase
FeO	0.10	0.00–0.30	0.10	hematite
MnO	0.17	0.03–0.42	0.12	spessartine
Al_2O_3	15.92	15.80–16.11	0.09	amblygonite
SiO_2	0.06	0.00–0.14	0.06	topaz
TiO_2	0.01	0.00–0.03	0.01	rutile
P_2O_5	21.94	21.72–22.15	0.15	apatite-(CaF)
F	21.35	19.60–23.60	1.55	topaz
H_2O	15.08	14.14–16.00	0.68	structure
O≡F	–8.99	–8.11 to –9.94	0.65	
Total	100.36	99.89–101.09	0.49	

among the average index of refraction, calculated density, and chemical composition. For galliskiite, the compatibility index is 0.004, indicating superior agreement among these data.

X-RAY CRYSTALLOGRAPHY AND STRUCTURE DETERMINATION

Both powder and single-crystal X-ray diffraction data were obtained on a Rigaku R-Axis Spider curved imaging plate microdiffractometer utilizing monochromatized Mo$K\alpha$ radiation. The powder data are presented in Table 2.

The Rigaku CrystalClear software package was used for processing the structure data. The SHELXL97 software (Sheldrick 2008) was used for the solution and refinement of the structure, which was solved by direct methods. Locating the Ca, Al, P, and O/F atoms was straightforward. Anions were assigned based upon bond-valence considerations. All anion sites with a bond-valence sum close to 1.0 were initially assumed to be F atoms. The chemical analysis indicated that these sites are likely to be occupied by $F_{7.23}(OH)_{0.77}$, however, the structure refinement provided no conclusive evidence (displacement parameters, refined occupancies, bond lengths, bond-valence sums) for assigning OH to any specific site. Consequently, the OH is assumed to be spread among the F sites, which were subsequently refined based upon occupancy by F alone. All cation and anion sites refined best at full occupancy.

With all non-hydrogen atoms located and refined with anisotropic displacement parameters, the refinement converged to R_1 = 3.66% and wR_2 = 8.68% for 3058 reflections with $F_o > 4\sigma F$. The difference map showed peaks assignable to all likely H atom positions associated with water molecules. These positions were refined with O(donor)-H distances restrained to 0.9 Å and the H-H distance corresponding to water molecules restrained to 1.45 Å, in each case with standard deviations of 0.03. Isotropic displacement parameters were held constant at 0.05 for all H atoms. In the final refinement, R_1 converged to 3.31% and wR_2 to 6.99%.

The details of the data collection and the final structure refinement are provided in Table 3. The final atomic coordinates and displacement parameters are in Table 4. Selected interatomic distances are listed in Table 5 and bond valences in Table 6. Table 7[1]. The observed and calculated structure factors (Table 7) and the CIF are on deposit[1].

DESCRIPTION AND DISCUSSION OF THE STRUCTURE

The structure of galliskiite consists of double chains of alternating corner-sharing AlF_3O_3 octahedra and PO_4 tetrahedra along the **a** axis (Fig. 2). Bonds to four distinct Ca atoms join the chains into a framework. Calcium atoms are also linked by

TABLE 2. X-ray diffraction data for galliskiite

I_{obs}	d_{obs}	d_{calc}	I_{calc}	*hkl*	I_{obs}	d_{obs}	d_{calc}	I_{calc}	*hkl*
70	7.904	7.896	40	011*	23	2.150	2.151	8	043*
		7.891	41	01$\bar{1}$*			2.150	7	11$\bar{5}$*
10	6.586	6.567	11	002	13	2.037	2.040	4	22$\bar{3}$
100	5.994	5.982	100	100*			2.035	6	13$\bar{4}$*
14	5.464	5.470	9	012*	14	1.9960	2.0017	4	026
		5.467	6	01$\bar{2}$			1.9966	3	31$\bar{1}$
15	5.179	5.227	7	111			1.9941	4	300
		5.179	4	110	14	1.9660	1.9671	15	31$\bar{3}$*
11	5.051	5.057	5	1$\bar{1}$0			1.9649	8	310
10	3.990	4.003	6	013	10	1.9040	1.9101	4	314
12	3.860	3.879	9	121			1.9035	4	24$\bar{1}$
13	3.792	3.776	10	12$\bar{1}$			1.8932	4	151
14	3.521	3.512	14	122*	15	1.8530	1.8581	5	31$\bar{1}$
58	3.280	3.284	63	004*			1.8504	4	15$\bar{1}$
30	3.113	3.117	4	014			1.8474	6	13$\bar{6}$
		3.115	6	01$\bar{4}$	27	1.8210	1.8234	8	036
		3.111	8	12$\bar{2}$			1.8222	11	03$\bar{6}$*
		3.107	14	12$\bar{3}$*	25	1.7980	1.7997	4	045
85	2.945	2.974	25	211			1.7984	4	04$\bar{5}$
		2.944	34	032*			1.7970	9	12$\bar{7}$*
		2.942	26	03$\bar{2}$	8	1.7300	1.7319	5	21$\bar{5}$
44	2.887	2.927	14	21$\bar{1}$			1.7282	3	325
		2.884	36	210*	7	1.6900	1.7088	4	227
		2.842	11	21$\bar{0}$			1.6859	4	251
8	2.650	2.654	4	221	8	1.6420	1.6459	4	060
		2.649	3	21$\bar{1}$			1.6418	2	008
20	2.483	2.494	8	20$\bar{2}$			1.6385	2	04$\bar{6}$
		2.491	6	214			1.6374	2	04$\bar{6}$
		2.481	9	223	6	1.5950	1.5995	2	161
6	2.430	2.427	6	22$\bar{3}$			1.5971	3	15$\bar{5}$
27	2.262	2.265	19	13$\bar{1}$	9	1.5790	1.5779	3	15$\bar{5}$
		2.260	14	23$\bar{2}$			1.5774	3	16$\bar{1}$
12	2.195	2.199	9	23$\bar{2}$*	7	1.5581	1.5566	2	31$\bar{7}$
		2.197	5	116			1.5563	3	34$\bar{1}$
		2.193	4	14$\bar{1}$	10	1.5157	1.5153	5	41$\bar{3}$
		2.189	4	006					
		2.187	5	11$\bar{6}$					

Notes: Only calculated reflections with intensities >10 are shown unless they correspond to observed reflections. Calculated *d*-spacings are based on the cell parameters refined from the powder data: a = 6.1879(6), b = 9.879(1), c = 13.581(2) Å, α = 89.55(1), β = 75.27(1), γ = 88.40(1)°.
* Reflections used for powder cell refinement.

[1] Deposit item AM-10-010, Table 7 and CIF. Deposit items are available two ways: For a paper copy contact the Business Office of the Mineralogical Society of America (see inside front cover of recent issue) for price information. For an electronic copy visit the MSA web site at http://www.minsocam.org, go to the *American Mineralogist* Contents, find the table of contents for the specific volume/issue wanted, and then click on the deposit link there.

TABLE 3. Data collection and structure refinement details for galliskiite

Diffractometer	Rigaku R-Axis Spider with curved imaging plate
X-ray radiation / power	Mo$K\alpha$ (λ = 0.71075 Å) / 50 kV, 40 mA
Temperature	298(2) K
Formula	$Ca_4Al_2(PO_4)_2F_8{\cdot}5H_2O$
Space group	$P\bar{1}$
Unit-cell dimensions	a = 6.1933(7) Å
	b = 9.871(1) Å
	c = 13.580(2) Å
	α = 89.716(3)°
	β = 75.303(4)°
	γ = 88.683(4)°
Z	2
Volume	802.9(2) Å^3
Density (for formula above)	2.674 g/cm^3
Absorption coefficient	1.813 mm^{-1}
F(000)	330
Crystal size	0.07 × 0.07 × 0.02 mm
θ range	3.10–27.47°
Index ranges	$-8 \le h \le 6$, $-12 \le k \le 12$, $-17 \le l \le 17$
Reflections collected / unique	16531 / 3633 [R_{int} = 0.045]
Reflections with $F_o > 4\sigma F$	3058
Completeness to θ = 27.46°	99.2%
Refinement method	Full-matrix least-squares on F^2
Parameters refined	293
GoF	1.049
Final R indices [$F_o > 4\sigma F$]	R_1 = 0.0331, wR_2 = 0.0699
R indices (all data)	R_1 = 0.0435, wR_2 = 0.0744
Largest diff. peak / hole	+0.42 / –0.61 e/A^3

Notes: $R_{int} = \Sigma|F_o^2 - F_c^2(\text{mean})|/\Sigma[F_o^2]$. GoF = $S = \{\Sigma[w(F_o^2 - F_c^2)^2]/(n-p)\}^{1/2}$. $R_1 = \Sigma||F_o| - |F_c||/\Sigma|F_o|$. $wR_2 = \{\Sigma[w(F_o^2 - F_c^2)^2]/\Sigma[w(F_o^2)^2]\}^{1/2}$. $w = 1/[\sigma^2(F_o^2) + (aP)^2 + bP]$ where a is 0.0241, b is 1.7689, and P is $[2F_c^2 + \text{Max}(F_o^2,0)]/3$.

Table 4. Atomic coordinates and displacement parameters (x 1000 Å^2) for galliskiite

	x	*y*	*z*	U_{eq}	U_{11}	U_{22}	U_{33}	U_{23}	U_{13}	U_{12}
Ca1	0.8349(1)	0.3009(1)	0.1467(1)	12(1)	18(1)	8(1)	9(1)	1(1)	−5(1)	0(1)
Ca2	0.9077(1)	0.2197(1)	0.6326(1)	10(1)	12(1)	9(1)	9(1)	−1(1)	−3(1)	1(1)
Ca3	0.9295(1)	0.4020(1)	0.3952(1)	10(1)	13(1)	9(1)	8(1)	0(1)	−3(1)	0(1)
Ca4	0.0304(1)	−0.1146(1)	0.1019(1)	9(1)	11(1)	8(1)	8(1)	0(1)	−3(1)	0(1)
Al1	0.8197(1)	0.4466(1)	0.8777(1)	6(1)	6(1)	6(1)	6(1)	1(1)	−2(1)	−1(1)
Al2	0.8282(1)	0.0602(1)	0.3749(1)	7(1)	8(1)	7(1)	6(1)	0(1)	−2(1)	1(1)
P1	0.7073(1)	−0.1122(1)	0.5813(1)	9(1)	9(1)	8(1)	9(1)	1(1)	−2(1)	0(1)
P2	0.2979(1)	0.3809(1)	0.9217(1)	8(1)	8(1)	8(1)	8(1)	−1(1)	−2(1)	0(1)
F1	0.9084(3)	0.1977(2)	0.2859(1)	13(1)	17(1)	12(1)	11(1)	4(1)	−5(1)	−2(1)
F2	0.7928(3)	0.1869(2)	0.4755(1)	12(1)	16(1)	9(1)	11(1)	−2(1)	−3(1)	−1(1)
F3	0.9303(3)	0.0990(2)	0.0714(1)	17(1)	32(1)	11(1)	10(1)	−1(1)	−6(1)	6(1)
F4	0.8895(3)	0.5611(2)	0.7708(1)	12(1)	14(1)	13(1)	8(1)	4(1)	0(1)	1(1)
F5	0.8421(3)	0.4283(2)	0.5697(1)	14(1)	16(1)	13(1)	13(1)	1(1)	−5(1)	−3(1)
F6	0.8873(3)	0.2998(2)	0.7936(1)	12(1)	18(1)	9(1)	10(1)	−3(1)	−4(1)	3(1)
F7	0.8888(3)	−0.0656(2)	0.2728(1)	11(1)	14(1)	11(1)	10(1)	−3(1)	−1(1)	0(1)
F8	0.7862(3)	0.3252(2)	0.9815(1)	11(1)	15(1)	10(1)	9(1)	3(1)	−4(1)	−1(1)
O1	0.4662(3)	−0.0688(2)	0.6330(2)	12(1)	11(1)	14(1)	13(1)	−2(1)	−3(1)	1(1)
O2	0.8644(3)	−0.0280(2)	0.6279(2)	10(1)	11(1)	10(1)	11(1)	−1(1)	−3(1)	1(1)
O3	0.7449(3)	−0.2654(2)	0.5967(2)	12(1)	11(1)	11(1)	15(1)	2(1)	−5(1)	−2(1)
O4	0.7656(3)	−0.0880(2)	0.4650(2)	10(1)	10(1)	9(1)	9(1)	1(1)	−2(1)	−2(1)
O5	0.2966(3)	0.2314(2)	0.8929(2)	12(1)	13(1)	8(1)	15(1)	−2(1)	−4(1)	0(1)
O6	0.5240(3)	0.4441(2)	0.8746(2)	12(1)	11(1)	13(1)	13(1)	1(1)	−3(1)	−1(1)
O7	0.1273(3)	0.4618(2)	0.8777(2)	9(1)	13(1)	9(1)	10(1)	0(1)	−4(1)	1(1)
O8	0.2315(3)	0.3934(2)	0.0397(2)	10(1)	12(1)	8(1)	10(1)	−2(1)	−5(1)	3(1)
OW1	0.5149(4)	0.2123(2)	0.6906(2)	17(1)	15(1)	18(1)	16(1)	−3(1)	−2(1)	−3(1)
OW2	0.2562(4)	0.3703(2)	0.5910(2)	20(1)	25(2)	16(1)	21(2)	−7(1)	−10(1)	5(1)
OW3	0.4542(4)	0.2256(2)	0.1561(2)	21(1)	22(2)	21(2)	20(2)	2(1)	−5(1)	2(1)
OW4	0.6224(4)	0.0450(3)	0.8914(2)	33(1)	17(2)	20(2)	65(3)	−1(2)	−19(2)	0(1)
OW5	0.6076(4)	0.4038(2)	0.3090(2)	18(1)	16(2)	14(1)	22(2)	0(1)	−3(1)	−1(1)
H1A	0.460(8)	0.212(4)	0.759(2)	50						
H1B	0.479(8)	0.130(3)	0.672(3)	50						
H2A	0.343(7)	0.328(5)	0.626(2)	50						
H2B	0.308(8)	0.354(5)	0.526(2)	50						
H3A	0.389(8)	0.233(5)	0.218(2)	50						
H3B	0.404(8)	0.274(4)	0.113(3)	50						
H4A	0.581(7)	−0.038(3)	0.887(4)	50						
H4B	0.503(6)	0.100(4)	0.903(4)	50						
H5A	0.554(7)	0.476(3)	0.287(4)	50						
H5B	0.490(6)	0.352(4)	0.340(3)	50						

Table 5. Selected bond distances (Å) and H-bond angles (°) for galliskiite

Ca1-F3	2.242(2)	Ca2-F5	2.292(2)	Ca3-F4	2.281(2)	Ca4-F3	2.250(2)
Ca1-F1	2.283(2)	Ca2-F6	2.301(2)	Ca3-F5	2.307(2)	Ca4-OW4	2.296(3)
Ca1-F8	2.349(2)	Ca2-OW1	2.362(2)	Ca3-F5	2.344(2)	Ca4-F3	2.309(2)
Ca1-O7	2.373(2)	Ca2-F2	2.439(2)	Ca3-O3	2.425(2)	Ca4-F7	2.312(2)
Ca1-OW3	2.461(3)	Ca2-O4	2.465(2)	Ca3-F2	2.450(2)	Ca4-O5	2.339(2)
Ca1-OW5	2.500(2)	Ca2-O2	2.470(2)	Ca3-OW2	2.487(2)	Ca4-F6	2.432(2)
Ca1-F4	2.668(2)	Ca2-F7	2.504(2)	Ca3-F1	2.536(2)	Ca4-F8	2.482(2)
Ca1-O8	2.694(2)	Ca2-OW2	2.590(3)	Ca3-OW5	2.555(3)	<Ca-O/F>	2.346
<Ca-O/F>	2.446	<Ca-O/F>	2.427	<Ca-O/F>	2.423		
Al1-F4	1.805(2)	Al2-F1	1.806(2)	P1-O1	1.532(2)	P2-O5	1.530(2)
Al1-F8	1.820(2)	Al2-F2	1.824(2)	P1-O2	1.546(2)	P2-O6	1.530(2)
Al1-F6	1.823(2)	Al2-F7	1.828(2)	P1-O3	1.547(2)	P2-O7	1.545(2)
Al1-O6	1.843(2)	Al2-O1	1.854(2)	P1-O4	1.547(2)	P2-O8	1.555(2)
Al1-O7	1.914(2)	Al2-O4	1.886(2)	<P-O>	1.543	<P-O>	1.540
Al1-O8	1.916(2)	Al2-O2	1.914(2)				
<Al-O/F>	1.853	<Al-O/F>	1.851				

D-H	*d*(D-H)	*d*(H···A)	<DHA	*d*(D···A)	A	<HDH
OW1-H1A	0.90(3)	1.85(3)	167(5)	2.741(3)	O5	103
OW1-H1B	0.90(3)	2.04(3)	167(5)	2.929(3)	O1	
OW2-H2A	0.90(3)	1.90(3)	171(5)	2.792(3)	OW1	110
OW2-H2B	0.87(3)	1.99(3)	146(5)	2.758(3)	O3	
OW3-H3A	0.84(3)	2.46(3)	171(5)	3.291(3)	O3	118
OW3-H3B	0.86(3)	2.00(3)	167(5)	2.850(4)	O8	
OW4-H4A	0.87(3)	1.98(3)	166(5)	2.830(4)	OW3	109
OW4-H4B	0.89(3)	1.82(3)	165(5)	2.696(3)	O5	
OW5-H5A	0.87(3)	2.48(3)	138(5)	3.174(3)	O6	107
OW5-H5B	0.91(3)	1.73(3)	175(5)	2.641(3)	O3	

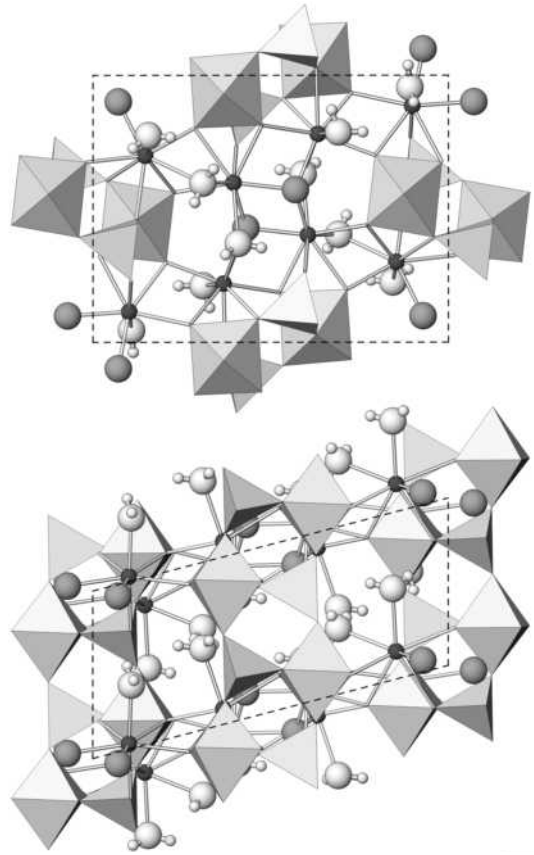

Figure 2. Crystal structure of galliskiite; views along **a** (**top**) and **b** (**bottom**). Calcium atoms are shown as small dark spheres, F atoms as large gray spheres, O atoms as large white spheres, and H atoms as small white spheres.

TABLE 6. Bond valence summations for galliskiite

	Ca1	Ca2	Ca3	Ca4	Al1	Al2	P1	P2	H1A	H1B	H2A	H2B	H3A	H3B	H4A	H4B	H5A	H5B	$\Sigma_a v$
F1	0.304		0.153			0.494													0.951
F2		0.199	0.193			0.470													0.863
F3	0.339			0.332	0.283														0.954
F4	0.107		0.305		0.495														0.908
F5		0.296	0.285	0.257															0.838
F6		0.289		0.203	0.472														0.964
F7		0.167		0.281		0.465													0.913
F8	0.254			0.177	0.476														0.907
O1						0.578	1.215			0.145									1.938
O2		0.257				0.491	1.170												1.918
O3			0.290				1.167					0.200	0.093					0.220	2.009
O4		0.260				0.530	1.167												1.957
O5				0.366				1.221	0.207							0.229			2.023
O6					0.595			1.221									0.104		1.921
O7	0.334				0.491			1.173											1.998
O8	0.140				0.489			1.142						0.167					1.937
OW1		0.344							0.793	0.855	0.187								2.178
OW2		0.187	0.245								0.813	0.800							2.046
OW3	0.263												0.907	0.833	0.173				2.177
OW4				0.411											0.827	0.771			2.009
OW5	0.237		0.204														0.896	0.780	2.077
$\Sigma_c v$	1.978	1.999	1.933	2.053	3.018	3.029	4.718	4.757	1.000	1.000	1.000	1.000	1.000	1.000	1.000	1.000	1.000	1.000	

Note: Non-hydrogen bond strengths from Brese and O'Keeffe (1991); hydrogen bond strengths from Ferraris and Ivaldi (1988), based on O-O distances; valence summations are expressed in valence units.

sharing isolated F atoms and H_2O molecules (Fig. 2).

The double-chain motif in the structure of galliskiite is distinct from that in any other known phosphate. The chain is similar to that in hannayite, $Mg_3(NH_4)_2(HPO_4)_4 \cdot 8H_2O$ (Catti and Franchini-Angela 1976); however, in hannayite the chains are further linked into a framework via additional tetrahedral–octahedral linkages. A similar chain is also found in synthetic trisodium iron phosphate (Hatert 2007), but in this structure additional PO_4 tetrahedra "decorate" the chain, sharing the outlying edges of the octahedra of the chain.

ACKNOWLEDGMENTS

Kimberly Tait and William D. Birch provided helpful reviews of the manuscript. This study was funded by the John Jago Trelawney Endowment to the Mineral Sciences Department of the Natural History Museum of Los Angeles County.

REFERENCES CITED

Brese, N.E. and O'Keeffe, M. (1991) Bond-valence parameters for solids. Acta Crystallographica, B47, 192–197.

Catti, M. and Franchini-Angela, M. (1976) Hydrogen bonding in the crystalline state. Structure of $Mg_3(NH_4)_2(HPO_4)_4(H_2O)_8$ (hannayite), and crystal chemical relationships with schertelite and struvite. Acta Crystallographica, B32, 2842–2848.

Colombo, F., Pannunzio Miner, E.V., Gay, H.D., Lira, R., and Dorais, M.J. (2007) Barbosalita y lipscombita en Cerro Blanco, Córdoba (Argentina): descripción y génesis de fosfatos secundarios en pegmatitas con triplita y apatita. Revista Mexicana de Ciencias Geológicas, 24, 120–130.

Dorais, M.J., Lira, R., Chen, Y., and Tingey, D. (1997) Origin of biotite-apatite-rich enclaves, Achala batholith, Argentina. Contributions to Mineralogy and Petrology, 130, 31–46.

Ferraris, G. and Ivaldi, G. (1988) Bond valence vs. bond length in O···O hydrogen bonds. Acta Crystallographica, B44, 341–344.

Galliski, M.A. (1999) Distrito pegmatítico Punilla. In E.O. Zappettini, Ed., Recursos Minerales de la República Argentina. Instituto de Geología y Recursos Minerales, SEGEMAR, Anales, 35, 547–550.

Galliski, M.A. and Černý, P. (2006) Geochemistry and structural state of columbite-group minerals in granitic pegmatites of the Pampean Ranges, Argentina. The Canadian Mineralogist, 44, 645–666.

Galliski, M.A., Černý, P., Márquez-Zavalía, M.F., and Chapman, R. (1999a) Ferrotitanowodginite, $Fe^{2+}TiTa_2O_8$, a new mineral of the wodginite group from the San Elias pegmatite, San Luis, Argentina. American Mineralogist, 84, 773–777.

Galliski, M.A., Cooper, M.A., Hawthorne, F.C., and Černý, P. (1999b) Bederite, a new pegmatite phosphate mineral from Nevados de Palermo, Argentina: description and crystal structure. American Mineralogist, 84, 1674–1679.

Hatert, F. (2007) Crystal structure of trisodium iron diphosphate, $Na_{2.88}Fe(PO_4)_2$, a synthetic phosphate with hannayite-type heteropolyhedral chains. Zeitschrift für Kristallographie, 222, 6–8.

Kampf, A.R., Colombo, F., and González del Tánago, J. (2010) Gayite, a new dufrénite-group mineral from the Gigante granitic pegmatite, Córdoba province, Argentina. American Mineralogist, 95, 384–389.

Lira, R. and Kirschbaum, A. (1990) Geochemical evolution of granites from the Achala Batholith of the Sierras Pampeanas, Argentina. In S.M. Kay and C.W. Rapela, Eds., Plutonism from Antarctica to Alaska, 241, p. 67–76. Geological Society of America, Special Paper, Boulder, Colorado.

Mandarino, J.A. (1981) The Gladstone-Dale relationship: Part IV. The compatibility concept and its application. The Canadian Mineralogist, 19, 441–450.

Rapela, C.W., Baldo, E.G.A., Pankhurst, R., and Fanning, C.M. (2008) The Devonian Achala batholith of the Sierras Pampeanas: F-rich, aluminous A-type granites. VI South American Symposium on Isotope Geology, Expanded abstract of 8 pages (CD), San Carlos de Bariloche.

Sheldrick, G.M. (2008) SHELXL97—Program for the refinement of crystal structures. University of Göttigen, Germany.

MANUSCRIPT RECEIVED SEPTEMBER 4, 2009
MANUSCRIPT ACCEPTED OCTOBER 8, 2009
MANUSCRIPT HANDLED BY ANTON CHAKHMOURADIAN